PHYSICAL REVIEW B **79**, 214422 (2009)

Distortion of the Stoner-Wohlfarth astroid by a spin-polarized current

Y. Henry*
Institut de Physique et Chimie des Matériaux de Strasbourg, CNRS, Université de Strasbourg, BP 43, F-67037 Strasbourg Cedex 2, France

S. Mangin and J. Cucchiara
Institut Jean Lamour, CNRS, Nancy Université, BP 239, F-54506 Vandoeuvre Cedex, France

J. A. Katine
Hitachi GST San Jose Research Center, 3403 Yerba Buena Road, San Jose, California 95135, USA

Eric E. Fullerton
Center for Magnetic Recording Research, University of California–San Diego, La Jolla, California 92093-0401, USA
(Received 23 January 2009; published 16 June 2009)

The Stoner-Wohlfarth astroid is a fundamental object in magnetism. It separates regions of the magnetic-field space with two stable magnetization equilibria from those with only one stable equilibrium and it characterizes the magnetization reversal of nanomagnets with uniaxial magnetic anisotropy induced by applied magnetic fields. On the other hand, it was recently demonstrated that transfer of spin angular momentum from a spin-polarized current provides an alternative way of switching the magnetization. Here, we examine the astroid of a nanomagnet under the combined influence of applied fields and spin-transfer torques. We find that spin transfer is most efficient at modifying the astroid when the external field is applied along the easy axis of magnetization. On departing from this situation, a threshold current appears below which spin transfer becomes ineffective yielding a current-induced dip in the astroid along the easy-axis direction. An extension of the Stoner-Wohlfarth model is outlined which accounts for this phenomenon.

DOI: 10.1103/PhysRevB.79.214422 PACS number(s): 75.75.+a, 72.25.−b, 75.60.−d, 85.75.−d

I. INTRODUCTION

The study of magnetization reversal has provoked continuous interest during the last 60 years. Indeed, this topic has proven to be scientifically very challenging and one of the fundamental issues in magnetic data storage and memory technologies. The difficulty to quantitatively understand magnetization reversal, known as Brown paradox,[1] results from complex domain patterns that can form in magnetic materials. However, for nanoscale systems the picture is greatly simplified, as initially described by Stoner and Wohlfarth[2] and Néel,[3] where the magnetic order parameter is assumed to be uniform across the dimensions of the sample and can be described as a single macrospin. 50 years were necessary to have the technological environment needed to test the macrospin model experimentally.[4] During that time, new techniques essential to fabricate and characterized nanometer-size objects such as scanning probe microscopies and nanolithography were developed. It was then demonstrated that, for some magnetic nanoparticles, the angular dependence of the switching field can indeed follow the famous Stoner-Wohlfarth (SW) astroid curve which separates regions of the cartesian magnetic-field space with two stable magnetic states from those with only one stable state.

Very few magnetic systems, however, possess the pure uniaxial magnetic anisotropy required to closely obey the Stoner-Wohlfarth model and the locus in the field space of all the magnetization switching fields of small magnets seldom take the shape of an astroid, as defined mathematically. However, over the years, the concept of Stoner-Wohlfarth astroid has been generalized to arbitrary effective anisotropy.[5] The term is now commonly used to refer to any critical surface that delimits the region of multistability of the magnetization in the field space and is a fundamental property of magnetic nanomaterials.

More recently, it has been theoretically predicted[6,7] and experimentally evidenced[8] that the injection of spin-polarized electrical currents can induce magnetization reversal. This new approach for magnetization reversal has generated considerable scientific interest and is expected to play a major role in many emerging spintronic technologies.[9] Usually, transfer of angular momentum from a spin-polarized current to the magnetization does not strongly modify the positions of the magnetization equilibria.[10] Its primary effect is to produce an extrinsic damping which either reinforces or opposes the intrinsic damping of the magnetization and modifies the stability of the equilibria rendering, for example, an unstable equilibrium stable. Spin transfer is expected to produce significant distortions of the astroid, making the region of bistability expand in some parts of the magnetic-field space and retract in others. This distortion was considered theoretically by Sun[11] in the case of an in-plane-polarized current acting on a magnet with a combination of uniaxial and easy-plane magnetic anisotropies.

In this paper, we examine how the Stoner-Wohlfarth astroid is indeed distorted by spin transfer in the simplest and most fundamental case of a nanomagnet with uniaxial magnetic anisotropy submitted to a current polarized along the easy axis. As we do this, we reveal how the efficiency of the spin-transfer torque with respect to magnetization switching

 ©2009 The American Physical Society

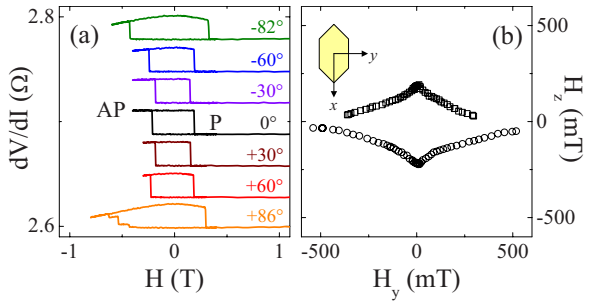

FIG. 1. (Color online) (a) Examples of differential resistance versus magnetic-field minor loops of the free element in a 100 nm×200 nm [Co/Ni]/Cu/[Co/Ni]/[Co/Pt] nanopillar recorded at different angles of the applied field with respect to the film normal. For clarity, the curves corresponding to field angles other than 0° are offset vertically. (b) Experimentally determined two-dimensional cross section of the zero-current astroid of the free element, in the (H_y, H_z) plane. Circles indicate a transition from the parallel (low-resistance) state to the antiparallel (high-resistance) state of the GMR device. Squares indicate the inverse transition.

varies in a rather counter-intuitive manner with the orientation of the external magnetic field.

II. EXPERIMENTS

The small magnet whose astroid is studied experimentally is the 3-nm-thick "free" element of a giant magnetoresistance (GMR) spin-valve patterned in the shape of a vertical pillar with 100 nm×200 nm hexagonal cross-sectional shape. Both the free element and the reference element of the device have perpendicular-to-plane magnetic anisotropy. This is achieved by using [Co/Ni] and [Co/Pt]/[Co/Ni] multilayer stacks, respectively, as described in details elsewhere.[12] In comparison with the intrinsic perpendicular-to-plane anisotropy of the extended Co/Ni multilayer, the shape anisotropy introduced in the plane by patterning the film in a noncircular pillar is negligible. Thus, the overall magnetic anisotropy of the free element is essentially *uniaxial* and its astroid should be in first approximation invariant upon rotation around the normal to the film plane $\hat{\mathbf{z}}$.

In practice, the astroid was built by determining the switching fields of the free element from differential resistance dV/dI versus magnetic-field minor hysteresis loops [Fig. 1(a)] recorded at varying field angle θ_H from $\hat{\mathbf{z}}$ ($-90° \leq \theta_H \leq +90°$), in the plane defined by $\hat{\mathbf{z}}$ and the small axis of the hexagon $\hat{\mathbf{y}}$ [see inset in Fig. 1(b)]. The differential resistance was measured using a Lakeshore Model 370 ac resistance bridge with an excitation current of 10 μA rms at 13.7 Hz. The dc current provided by a Keithley Model 2400 sourcemeter was injected in the sample using a home-made bias-T interface. Before measuring each magnetoresistance loop, a positive field in excess of 1 T was applied to ensure that both the free element and the reference element would be initially magnetized positively, i.e., in the $z>0$ semispace. The experiments have been performed several times and no strong fluctuation of the switching fields, i.e., a stochastic behavior related to thermal fluctuations, was observed. Moreover, no signature of spin-transfer-induced steady precession states, i.e., nonhysteretic peaks or dips in the differential resistance versus field loops,[12] was found with the dc current values used.

In the off-axis geometries ($\theta_H \neq 0$), the magnetization vectors of the two elements do not always remain strictly collinear to each other during field cycling. This manifests in the curvature of both the lower branch and, more obviously, the upper branch of the measured GMR loops [Fig. 1(a)]. However, for the sake of simplicity, we will still name the low-resistance state and the high-resistance state of the nanopillar the "parallel" (P) state and the "antiparallel" (AP) state, respectively. Three dimensional micromagnetic simulations performed with the OOMMF software package[13] indicate that the continuous change in the relative orientation of the magnetization vectors that the curvature reveals is primarily ascribable to the rotation of the magnetization of the free layer. To a good approximation, the magnetization of the reference layer, harder magnetically, remains fixed. An unambiguous determination of the switching fields $H_{\mathrm{AP}\to P}$ and $H_{P\to\mathrm{AP}}$ was possible only for field angles such that $|\theta_H| < +85°$, where the reversals of the free-element magnetization occur abruptly. For $85° \leq |\theta_H| \leq 88°$, the GMR loops may contain several well-separated jumps [bottommost loop in Fig. 1(a)] indicating that the reversal is nonuniform and sequential either because it becomes dominated by pinning of domain walls on defects or, equally likely, for intrinsic micromagnetic reasons such as the bifurcations discussed in Ref. 14. For $|\theta_H| > 88°$, finally, sharp discontinuities are no longer visible in the experimental curves. Hereafter, we limit our discussion to angles less than 85°.

The zero-current astroid of the free element is shown in Fig. 1(b). It is qualitatively similar to the astroid of an isolated single-domain particle. However, two differences may be pointed out. (i) First, the experimental astroid is comparatively flatter: the switching field close to the hard axis is markedly larger than that along the easy axis. This is an indication that the lateral dimensions of the free element are too large for truly coherent rotation of the magnetization to occur throughout the entire range of angles explored. Indeed, in the literature, demonstrations of coherent rotation behavior exist only for smaller magnetic objects.[4] Full micromagnetic simulations reproduce this flattening and show that, in the parallel state, an S-like nonuniform magnetization pattern forms in the free layer at large field angles. (ii) Second, unlike the square astroid of a Stoner particle, the astroid of the free element shows a significant asymmetry with respect to the hard axis of magnetization. This is due to the sizable dipolar coupling that exists between the two magnetic elements of the pillar only separated by a 4-nm-thick copper spacer. The reference element magnetized along $\hat{\mathbf{z}}$ produces an average stray field of about 25 mT which tends to maintain the magnetization of the free element oriented upwards. This results in a displacement of the astroid towards negative H_z, quite as for an exchange-biased ferromagnetic film.[15]

We now extend these studies to include the contribution of spin-polarized currents to reversal. To avoid damage of the nanopillar during measurements, we have had to limit our investigations to moderate current densities ($|j| \leq 6 \times 10^{11}$ A/m^2). Moreover, the system studied behaves in such a way[12] that positive currents which become spin po-

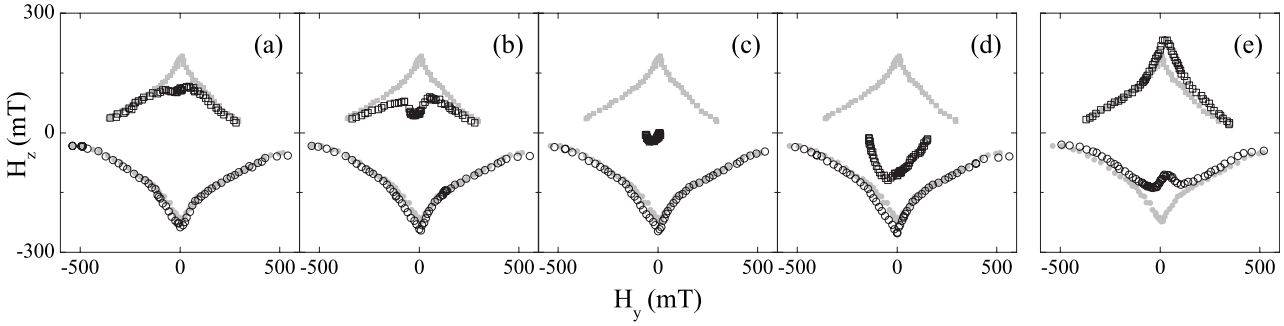

FIG. 2. Experimentally determined astroids of the free element in a 100 nm×200 nm [Co/Ni]/Cu/[Co/Ni]/[Co/Pt] nanopillar for varying values of the dc current density: (a) $j=+2\times10^{11}$ A/m^2, (b) $+3\times10^{11}$ A/m^2, (c) $+4\times10^{11}$ A/m^2, (d) $+6\times10^{11}$ A/m^2, and (e) -6×10^{11} A/m^2. The zero-current astroid is also shown for comparison (solid gray symbols).

larized by transmission through the reference layer are much more efficient at modifying the switching fields of the free element (especially $H_{\mathrm{AP}\to P}$) than negative ones polarized on reflection from the reference layer. Therefore, we are mainly presenting here results obtained with positive currents.

Positive currents favor an alignment of the free-element magnetization parallel to that of the reference element. As may be seen in Figs. 2(a)–2(d), the spin-transfer effect they generate modifies strongly the upper half of the astroid, that is, the part of the critical curve corresponding to the switching from the antiparallel state to the parallel state ($H_{\mathrm{AP}\to P}$). As spin-transfer starts to operate, the easy-axis cusp present for zero dc current [Fig. 1(b)] disappears. Instead, a dip forms along the easy-axis direction which gets deeper and broader as the current increases. At first, the large angle parts of the $H_{\mathrm{AP}\to P}$ branch of the astroid remains relatively unchanged [Figs. 2(a) and 2(b)]. At larger currents, the entire branch which can be probed with radial fields (constant θ_H) is affected and takes a semicircular shape [Figs. 2(c) and 2(d)]. In contrast, the lower half of the astroid corresponding to the reversal from the parallel state to the antiparallel state ($H_{P\to\mathrm{AP}}$) is not strongly affected under positive current. The domain of stability of the parallel state only slightly expands in the direction of negative H_z and the easy-axis cusp remains visible.

For negative currents [Fig. 2(e)], a qualitatively symmetrical behavior is observed. On the side of the $H_{P\to\mathrm{AP}}$ branch, the astroid shrinks back as a dip forms along the easy-axis direction. On the side of the $H_{\mathrm{AP}\to P}$ branch, the astroid noticeably expands towards positive H_z. Quantitative differences exist though (e.g., the size of the dip) between astroids obtained for currents of the same magnitude but opposite polarities [compare Figs. 2(d) and 2(e)]. These are straightforwardly related to the difference in the spin-transfer efficiency between the two current directions. The fact that upon injection of currents of the two polarities, large parts of the critical curve, and sometimes one half of it, remain virtually unchanged is a strong indication that the heat and Oersted field generated by passing the current through the device are not sufficient to modify the astroid and cannot be evoked to account for the observed distortions.[16]

In the remainder of the paper, we will mostly concentrate on those parts of the astroid where spin transfer gives rise to a reduction in the switching field, that is, in those regions where the dip forms, which are the most relevant to technological applications. Theoretical investigations[17] have shown that in the on-axis geometry ($\theta_H=0$), linear relations should exist between the values of $H_{P\to\mathrm{AP}}$ and $H_{\mathrm{AP}\to P}$ and the magnitude of the dc current injected, in partial agreement with experimental findings.[12] The present results reveal that such is not the case if the field is applied at a large angle away from the easy axis. More specifically, for every nonzero field angle, a threshold current j_{min} exists below which spin transfer does not affect magnetization reversal. This minimum current increases with increasing θ_H. As a consequence for *moderate* current values, there exist a field angle θ_H^{max} above which spin transfer becomes ineffective. These results are rather counterintuitive. Indeed, as θ_H increases, so does the relative angle between the magnetization vectors of the reference and free layers and, consequently, so does the spin-transfer torque. Naively, one might therefore expect an enhanced efficiency of spin transfer at large field angle.

III. NUMERICAL SIMULATIONS

To gain a deeper understanding of the effect of spin transfer on the astroid, we carried out numerical simulations in a macrospin approach where the magnetization of the reference layer is supposed to be fixed. By comparing the experimental results with those from such a model, our goal is to unravel what is intrinsic to the physics of spin transfer and what is possibly due to sample imperfections, higher-order magnetic anisotropies or deviations from a uniform magnetization distribution.

In order to include a description of the dipolar interactions in the system as realistic as possible under the assumption of uniform magnetization, the two magnetic elements of the nanopillar were assumed to be identical, 200-nm-long, 100-nm-wide, and 3-nm-thick parallelepipeds, separated vertically by 4 nm. Analytical results from Newell *et al.*[18] were used to calculate two tensors; first, the self-demagnetizing tensor N_D, which relates the demagnetizing field $\mathbf{H}_i^D$ inside parallelepiped i to its magnetization $\mathbf{M}_i$ through $\mathbf{H}_i^D = -N_D \cdot \mathbf{M}_i$,

$$N_D = \begin{vmatrix} 0.0213 & 0 & 0 \\ 0 & 0.0437 & 0 \\ 0 & 0 & 0.9350 \end{vmatrix}, \quad (1)$$

and second, the so-called mutual demagnetizing tensor N_M which allows one to give a simple expression for the stray

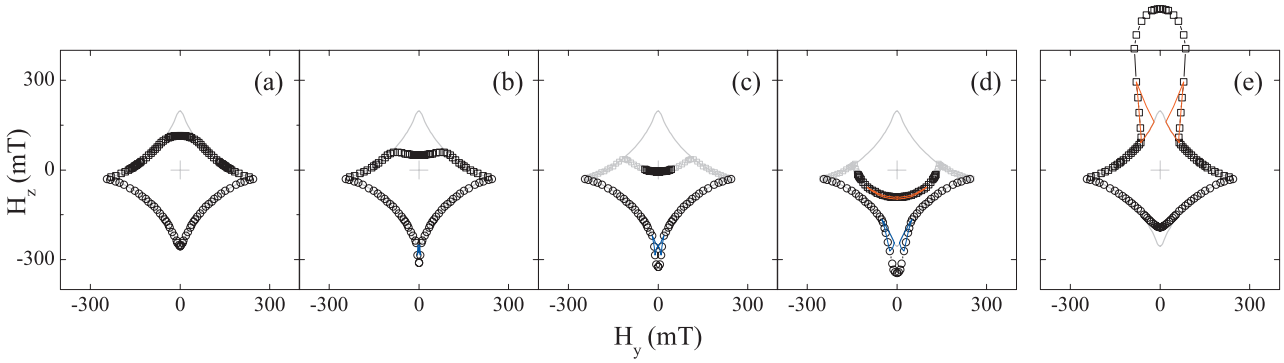

FIG. 3. (Color) Calculated astroids of the free element. The values of the dc current density used in the simulations are the same as experimentally (Fig. 2): (a) $j=+2\times10^{11}$ A/m^2, (b) $+3\times10^{11}$ A/m^2, (c) $+4\times10^{11}$ A/m^2, (d) $+6\times10^{11}$ A/m^2, and (e) -6×10^{11} A/m^2. The large black symbols indicate the portions of the astroid accessible upon sweeping the magnetic field at constant θ_H. The smaller gray symbols are the complementary parts determined from field sweeps at constant H_y. The thin red (respectively, blue) lines delineate regions of the field space where the stationary antiparallel state (respectively, parallel state) is replaced by a steady precession state with large negative (respectively, positive) m_z. The astroid computed for $j=0$ is also shown for comparison (gray line).

field $\mathbf{H}_i^{\mathrm{dip}}$ generated by element j (magnetization $\mathbf{M}_j$) and experienced by element i, $\mathbf{H}_i^{\mathrm{dip}}=-N_M\cdot\mathbf{M}_j$,

$$N_M=\begin{vmatrix} 0.0105 & 0 & 0 \\ 0 & 0.0217 & 0 \\ 0 & 0 & -0.0322 \end{vmatrix}. \tag{2}$$

Both the demagnetizing field $\mathbf{H}^D$ and the stray field from the reference element $\mathbf{H}^{\mathrm{dip}}$ were included in the effective field acting the magnetization of the free element. For the latter element, we assumed a saturation magnetization of $M_S=650$ kA/m, a perpendicular-to-plane magnetic anisotropy constant $K_\perp=3\times10^5$ J/m^3 and a damping parameter $\alpha=0.01$, whereas for the reference element we used $M_S^{\mathrm{ref}}=500$ kA/m.[12]

The switching fields were extracted from magnetization versus field loops calculated by solving numerically, with the fourth-order Runge-Kutta algorithm, a modified Landau-Lifschitz-Gilbert (LLG) equation including an additional spin-transfer torque acting on the magnetization $\mathbf{M}$ of the form proposed by Slonczewski,[6,19] that is, $-\beta(\theta)j/M_S[\mathbf{M}\times(\mathbf{M}\times\hat{\mathbf{p}})]$, with the direction of spin polarization $\hat{\mathbf{p}}=\hat{\mathbf{z}}$. The variation of the spin-transfer efficiency function β with the relative angle θ between $\hat{\mathbf{p}}$ and the magnetization direction $\hat{\mathbf{m}}=\mathbf{M}/M_S$ assumed in these calculations is of the same form as that found in Ref. 20,

$$\beta(\hat{\mathbf{m}}\cdot\hat{\mathbf{p}})=\frac{\gamma\hbar}{2d\mu_0M_Se}\left[\frac{q_+}{b_0+b_1(\hat{\mathbf{m}}\cdot\hat{\mathbf{p}})}+\frac{q_-}{b_0-b_1(\hat{\mathbf{m}}\cdot\hat{\mathbf{p}})}\right], \tag{3}$$

where d is the thickness of the free layer, $\gamma>0$ is the gyromagnetic ratio, and $e>0$ is the absolute value of the electron charge. The parameters $q_+=1/60$, $q_-=-1/600$, $b_0=1$, and $b_1=1/2$ were chosen in the following way. b_0 was arbitrarily set to 1. The ratio b_0/b_1 was set to 2 so as to obtain a significant asymmetry of the slope of the spin-transfer torque between angles θ close to 0° and those close to 180°. The ratio q_+/q_- was set to -10 to account for the asymmetry of the GMR device architecture. Finally, the ratio $b_0/q_+=60$ was adjusted so that values of the current density used in the simulations would approximately match those in the experiments.

No effort was made to adjust these parameters further in order to get the best possible agreement with experimental data and reach a quantitative agreement, should this be possible. Yet, as may be seen in Fig. 3, most of the important features of the spin-transfer-distorted astroid discussed before are accounted for by this approach. In particular, the existence of a threshold current when $\theta_H\neq0$ is confirmed. This is even more clearly seen in Fig. 4(a) which plots the change in the switching field $\Delta H_{\mathrm{AP}\to P}(j,\theta_H)=H_{\mathrm{AP}\to P}(j,\theta_H)-H_{\mathrm{AP}\to P}(0,\theta_H)$ as a function of the current density, for various field orientations. Also obvious from Fig. 4(a) is that the larger θ_H the less linear the variation of the switching field with j, beyond $j_{\min}$. Figure 4(b) illustrates the loss of efficiency of spin transfer beyond an angle $\theta_H^{\max}$ which increases with increasing j.

The absence of a large bubble-shaped extension of the astroid along the H_z axis, for negative current, is the only important point of disagreement between modeling [Fig. 3(e)] and experiments [Fig. 2(e)]. Numerically, the extent of this protusion is found to be strongly reduced if the easy axis of magnetization makes an angle of a few degrees with respect to the magnetic-field plane. A slight distribution in the orientation of the easy axis in the free layer of the studied device is thus a possible explanation for the discrepancy. We note however that the choice of the spin-transfer efficiency function β affects also the size of this bubble.

IV. ANALYTICAL MODELING

Interestingly, a simple extension of the Stoner-Wohlfarth model[2] is sufficient to capture most features of the current-distorted astroid. Let us consider a uniformly magnetized nanomagnet with saturation magnetization M_S and uniaxial magnetic anisotropy of axis $\hat{\mathbf{z}}$ and constant K ($H_K=2K/\mu_0M_S$). Its magnetization $\mathbf{M}=M_S\hat{\mathbf{m}}$ is described by a polar angle θ measured from $\hat{\mathbf{z}}$ and an azimuthal angle ϕ

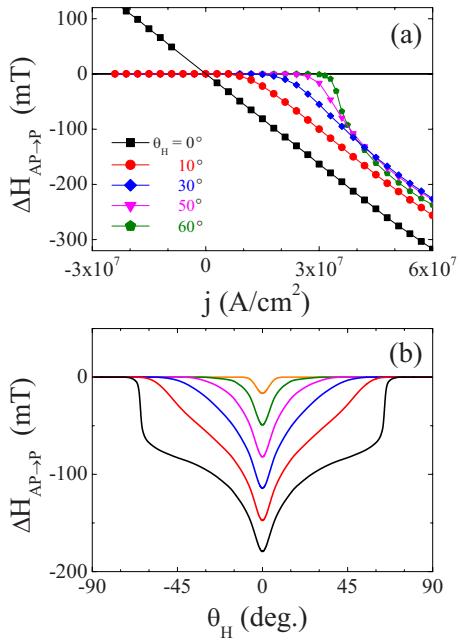

FIG. 4. (Color online) Calculated change in the switching field for the transition from the AP state to the P state. (a) $\Delta H_{\mathrm{AP}\to P}(j,\theta_H)=H_{\mathrm{AP}\to P}(j,\theta_H)-H_{\mathrm{AP}\to P}(0,\theta_H)$ versus current density j for various values of the applied field angle θ_H. (b) $\Delta H_{\mathrm{AP}\to P}$ versus field angle θ_H for equally spaced values of the current density j ranging from $+0.6\times10^{11}$ A/m^2 (topmost, orange curve) to $+3.6\times10^{11}$ A/m^2 (bottom-most black curve).

measured from $\hat{\mathbf{x}}$ (Fig. 5). As is the case experimentally, let us assume that the external field is applied in the yz plane. In the orthonormal direct basis formed by the three vectors $\hat{\mathbf{m}}$, $\hat{\mathbf{e}}_\theta=\partial\hat{\mathbf{m}}/\partial\theta$, and $\hat{\mathbf{e}}_\phi=(1/\sin\theta)\partial\hat{\mathbf{m}}/\partial\phi$, the modified LLG equation that governs the dynamics of $\hat{\mathbf{m}}$ may be written as

$$\frac{d\hat{\mathbf{m}}}{dt}=-\gamma(\hat{\mathbf{m}}\times\mathbf{H}^*_{\mathrm{eff}})+\alpha\left(\hat{\mathbf{m}}\times\frac{d\hat{\mathbf{m}}}{dt}\right), \tag{4}$$

where α is Gilbert damping constant. The total effective field acting on $\mathbf{M}$,

$$\mathbf{H}^*_{\mathrm{eff}}=\mathbf{H}+H_K(\hat{\mathbf{m}}\cdot\hat{\mathbf{z}})\hat{\mathbf{z}}+j\frac{\beta(\hat{\mathbf{m}}\cdot\hat{\mathbf{z}})}{\gamma}(\hat{\mathbf{m}}\times\hat{\mathbf{p}}) \tag{5}$$

is the sum of the usual effective field

$$\mathbf{H}_{\mathrm{eff}}=-\frac{1}{\mu_0 M_S}\frac{\partial E}{\partial\hat{\mathbf{m}}} \tag{6}$$

which derives from the magnetic energy

$$E=-\mu_0\mathbf{M}\cdot\mathbf{H}-K(\hat{\mathbf{m}}\cdot\hat{\mathbf{z}})^2 \tag{7}$$

and of the spin-torque field

$$\mathbf{H}_{\mathrm{ST}}=j\frac{\beta}{\gamma}(\hat{\mathbf{m}}\times\hat{\mathbf{z}})=-j\frac{\beta}{\gamma}\sin\theta\,\hat{\mathbf{e}}_\phi. \tag{8}$$

At equilibrium, $\hat{\mathbf{m}}$ is necessarily parallel to $\mathbf{H}^*_{\mathrm{eff}}$. Therefore, the equilibrium conditions are

$$(\mathbf{H}^*_{\mathrm{eff}}\cdot\hat{\mathbf{e}}_\theta)_0=0 \tag{9a}$$

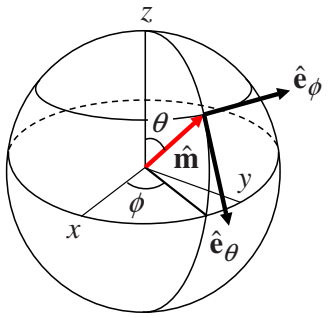

FIG. 5. (Color online) Polar and azimuthal angles θ and ϕ, and vector basis $\{\hat{\mathbf{m}},\hat{\mathbf{e}}_\theta,\hat{\mathbf{e}}_\phi\}$.

$$(\mathbf{H}^*_{\mathrm{eff}}\cdot\hat{\mathbf{e}}_\phi)_0=0, \tag{9b}$$

where the subscript "0" denotes equilibrium.

The consequence of introducing spin transfer is twofold. (i) First, since $\mathbf{H}^*_{\mathrm{eff}}$ may have a component along $\hat{\mathbf{e}}_\phi$ [Eqs. (5) and (8)], $\hat{\mathbf{m}}$ does not always lie in the plane defined by the applied field $\mathbf{H}$ and the easy axis $\hat{\mathbf{z}}$, at equilibrium. Therefore, the problem becomes three dimensional, in general. In the limit of small currents (and/or small field angles), however, deviations of $\hat{\mathbf{m}}$ from the $(\hat{\mathbf{z}},\mathbf{H})$ plane remain small and, in first-order approximation, the problem can still be treated as if it were two-dimensional ($\phi=\pi/2$). (ii) Second, the stability of the equilibria can no longer be determined from free-energy considerations only and a new stability criterion must be derived. This is possible analytically in the small current limit. Indeed, performing a linear stability analysis around an equilibrium position θ_0, i.e., relating stability to the gradient of the total torque along $\hat{\mathbf{e}}_\theta$, leads to the criterion

$$\frac{\partial}{\partial\theta}\left[\alpha(\mathbf{H}_{\mathrm{eff}}\cdot\hat{\mathbf{e}}_\theta)-j\frac{\beta(\theta)}{\gamma}\sin\theta\right]\Bigg|_{\theta=\theta_0}\leq 0. \tag{10}$$

The above criterion is written so as to reveal the competition between two terms related to the torques produced by the effective field $\mathbf{H}_{\mathrm{eff}}$ and the spin-torque field $\mathbf{H}_{\mathrm{ST}}$, respectively. More practically, Eq. (10) shows also that stability in the off-axis case ($\theta_H\neq0,\theta_0\neq0[\pi]$) is influenced not only by the spin-transfer efficiency function $\beta(\theta)$ but also by its derivative $\partial\beta/\partial\theta$, a point first put forward by Smith *et al.*[21]

By combining the equilibrium condition [Eq. (9)] and the stability criterion [Eq. (10)], we can derive the following parametric equations of the astroid under small current:

$$\begin{cases}H_y=H_K\sin^3\theta_0-j\sin\theta_0 C(\theta_0)\\ H_z=-H_K\cos^3\theta_0-j\cos\theta_0 C(\theta_0)\end{cases} \tag{11}$$

with

$$C(\theta_0)=\frac{1}{\alpha\gamma}\left.\frac{\partial(\beta\sin\theta)}{\partial\theta}\right|_{\theta=\theta_0}, \tag{12}$$

where the correction terms due to spin transfer appear most clearly. As may be seen in Figs. 6(a) and 6(b) predictions from this analytical model regarding the stability of the equilibria closely agree with results from computer simulations using the same assumptions. Of course, the model is unable to predict the existence of dynamic states and regions of the

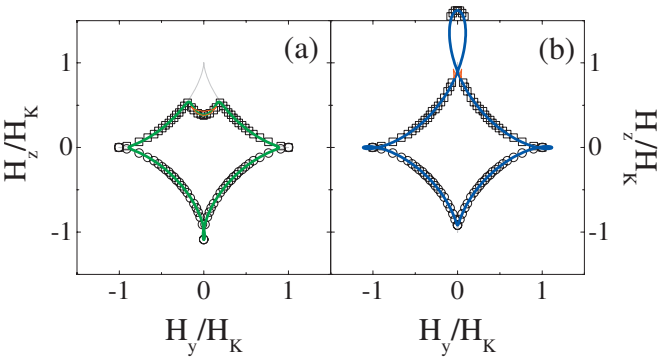

FIG. 6. (Color) Comparison of astroids drawn from the extended Stoner-Wohlfarth model [Eqs. (11) and (12)] (thick lines) and deduced from macrospin simulations (symbols) in the case of a small positive current, (a) $j=+3\times10^9$ A/m^2 and a small negative current, (b) $j=-3\times10^9$ A/m^2. As in Fig. 3, the thin red lines delineate regions of the field space where the antiparallel state is replaced by a steady precession state with large negative m_z.

field space where two magnetic states exist but only one is stationary (as indicated by numerical simulations) are not comprised in the astroid thus defined. In the extended SW model, the negative counterpart of the dip is a kind of protruding bubble attached to the rest of the astroid through a crunode [double point, Fig. 6(b)].

For the numerical application of Eq. (11) and the comparative macrospin simulations shown in Fig. 6, the overall magnetic-anisotropy constant K was set to $K_\perp-\mu_0 M_S/2$ with the values of $K_\perp$ and M_S given in Sec. III. Moreover, we used an expression of β in agreement with Slonczewski original proposition[6]

$$\beta(\hat{\mathbf{m}}\cdot\hat{\mathbf{p}})=\frac{\gamma\hbar}{2d\mu_0 M_S e}\left[\frac{1}{f(P)(3+\hat{\mathbf{m}}\cdot\hat{\mathbf{p}})-4}\right] \tag{13}$$

with

$$f(P)=\frac{(1+P)^3}{4P^{3/2}} \tag{14}$$

and a degree of spin polarization of the electrons coming out of the reference layer arbitrarily set to $P=50\%$. For demonstration purposes, this function was deliberately chosen different from the one used in the numerical simulations of Fig. 3 [Eq. (3)] although both are monotonous, increasing functions of θ on the $[0,\pi]$ interval. Yet, the two functions which were previously considered in the literature lead to qualitatively identical modifications of the astroid shape and to the existence of an angle $\theta_H^{\max}$ above which the switching field is virtually unchanged. This demonstrates once more the robustness of this feature.

V. DISCUSSION

The magnitude of the effective field acting on the magnetization at the very beginning of reversal is the key parameter to consider in order to understand the effect of spin transfer on the astroid. The reason for that is that H_{eff} is a measure of the intrinsic damping. Indeed, the larger H_{eff}, the faster the precession of $\mathbf{M}$ around $\mathbf{H}_{\text{eff}}$, in the event of an excursion away from the equilibrium, and the stronger the viscous damping which drives $\mathbf{M}$ back to equilibrium. From Eqs. (9) and (10), one can readily derive that along the zero-current astroid

$$H_{\text{eff}}(\theta_0)=H_K\sin^2\theta_0. \tag{15}$$

The on-axis geometry is extremely particular. In this geometry, the effective field and the intrinsic damping vanish at the zero-current switching fields [Eq. (15)]. This is why, close to these field values, any small amount of extrinsic damping brought in by spin transfer affects the magnetization reversal. Furthermore, the orientation of the magnetization being independent of the applied field ($\theta_0=0$ or π), H_{eff} varies linearly with H and the extrinsic damping due to spin transfer is just proportional to j. This leads to the observed linear relation between the switching field and the injected current [Fig. 4(a)].

In the off-axis geometries, the situation is qualitatively different. Indeed, the effective field always retains a sizable magnitude and the magnetization experiences a finite intrinsic (positive) damping at reversal. To induce an early switching of the magnetization, e.g., $H_{\text{AP}\to P}(j)<H_{\text{AP}\to P}(0)$, spin transfer must produce enough negative damping to overcome this finite intrinsic damping. $j_{\min}$ is the smallest current density which realizes this. If j is less than $j_{\min}$ then, irrespective of j, reversal occurs when the equilibrium loses its local stability, i.e., upon crossing (exiting) the zero-current astroid, as for $j=0$. The mathematical complexity of the $\theta_H\neq0$ case, which is largely due to the fact that the orientation of the magnetization changes continuously with H, makes it difficult to derive an analytical expression for the dependence of $j_{\min}$ on θ_H. To explain why $j_{\min}$ increases with θ_H or, equivalently, why a moderate current density generates enough negative damping only up to a given field angle $\theta_H^{\max}$ one has to invoke the fact that the intrinsic (positive) damping increases faster with θ_H than the extrinsic (negative) one.

VI. CONCLUSION

In summary, we have investigated the effect of spin transfer on the Stoner-Wohlfarth astroid of a small magnet with uniaxial magnetic anisotropy. The distortions observed experimentally are well accounted for qualitatively by both macrospin numerical simulations and a simple extension of the SW analytical model. Evidence has been given that spin transfer is more efficient at modifying the switching field in geometries close to the so-called axial geometry[17] where the external field is applied along the easy-axis and spin-polarization direction. On departing form this situation, a threshold current appears below which spin transfer is ineffective, the larger the field angle the larger this current.

Our results have implications for solid-state device applications. For zero current, the SW model predicts that a twofold reduction in the switching field can be achieved by applying the external field at an angle of 45° from the anisotropy axis, a strategy often used in magnetic-memory cells. What our results suggest is that combining such a strategy with spin transfer will not necessarily help in reducing

the switching field further. For the injection of current to be efficient, its density will have to exceed the threshold value j_{min}. We note finally that the physics which describes the distortions of the Stoner-Wohlfarth astroid under the influence of spin-polarized currents is similar to that which explains spin-transfer-induced instabilities of the sensing layer in GMR read heads of hard-disk drives.[21]

ACKNOWLEDGMENTS

The authors thank M. Bailleul, E. Bonet, J. Grollier, A. D. Kent, P. Panissod, D. Ravelosona, J. Sun, A. Thiaville, C. Thirion, and I. Tudosa for insightful discussions as well as O. Bengone for assistance in symbolic computations.

*yves.henry@ipcms.u-strasbg.fr

[1] W. F. Brown, Jr., Rev. Mod. Phys. **17**, 15 (1945).
[2] E. C. Stoner and E. P. Wohlfarth, Philos. Trans. R. Soc. London, Ser. A **240**, 599 (1948); reprinted in IEEE Trans. Magn. **27**, 3475 (1991).
[3] L. Néel, Ann. Geophys. **5**, 99 (1949).
[4] E. Bonet, W. Wernsdorfer, B. Barbara, A. Benoit, D. Mailly, and A. Thiaville, Phys. Rev. Lett. **83**, 4188 (1999).
[5] A. Thiaville, Phys. Rev. B **61**, 12221 (2000).
[6] J. C. Slonczewski, J. Magn. Magn. Mater. **159**, L1 (1996).
[7] L. Berger, Phys. Rev. B **54**, 9353 (1996).
[8] J. A. Katine, F. J. Albert, R. A. Buhrman, E. B. Myers, and D. C. Ralph, Phys. Rev. Lett. **84**, 3149 (2000).
[9] J. A. Katine and E. E. Fullerton, J. Magn. Magn. Mater. **320**, 1217 (2008).
[10] A. N. Slavin and V. S. Tiberkevich, Phys. Rev. B **72**, 094428 (2005).
[11] J. Z. Sun, Phys. Rev. B **62**, 570 (2000).
[12] S. Mangin, D. Ravelosona, J. A. Katine, M. J. Carey, B. D. Terris, and E. E. Fullerton, Nature Mater. **5**, 210 (2006).
[13] M. J. Donahue and D. G. Porter, OOMMF User's Guide, version 1.0. Interagency Report No. NISTIR 6376, 1999 (unpublished).
[14] O. Fruchart, J.-C. Toussaint, P.-O. Jubert, W. Wernsdorfer, R. Hertel, J. Kirschner, and D. Mailly, Phys. Rev. B **70**, 172409 (2004).
[15] L. Spinu, Al. Stancu, Y. Kubota, G. Ju, and D. Weller, Phys. Rev. B **68**, 220401(R) (2003).
[16] M. Jamet, W. Wernsdorfer, C. Thirion, D. Mailly, V. Dupuis, P. Mélinon, and A. Pérez, Phys. Rev. Lett. **86**, 4676 (2001).
[17] Y. B. Bazaliy, B. A. Jones, and S.-C. Zhang, Phys. Rev. B **69**, 094421 (2004).
[18] A. J. Newell, W. Williams, and D. J. Dunlop, J. Geophys. Res. **98**, 9551 (1993).
[19] J. C. Slonczewski, J. Magn. Magn. Mater. **247**, 324 (2002).
[20] M. D. Stiles and J. Miltat, in *Spin Dynamics in Confined Magnetic Structures, III*, edited by B. Hillebrands and A. Thiaville (Springer, Berlin, 2006), pp. 225–308.
[21] N. Smith, J. A. Katine, J. R. Childress, and M. J. Carey, IEEE Trans. Magn. **41**, 2935 (2005).